Synthetic image generation of chemical plumes for hyperspectral applications

S. Didi Kuo
John R. Schott
Chia Y. Chang
Rochester Institute of Technology
Center for Imaging Science
1 Lomb Memorial Drive
Rochester, New York 14623

Abstract. Remote sensing of factory stack plumes may provide unique information on the constituents of the plume. Potential information on the chemical composition of the factory products may be gathered from thermal emission/absorption in the infrared. We have developed a new model for generating synthetic images of plumes as viewed from a hyperspectral sensor using DIRSIG, a radiometrically based ray-tracing code. Existing plume models that describe the characteristics of the plume (constituents, concentration, and temperature) are used for input into DIRSIG. Ray-tracing is done for the scene that accounts for radiance from the plume, atmosphere and background, as well as any transmissive effects. Observations are made on the interaction between the plume and its background and possible effects for remote sensing. Images of gas plumes using a hyperspectral sensor are illustrated. Several sensitivity studies are done to demonstrate the effects of changes in plume characteristics on the resulting image. Inverse algorithms that determine the plume effluent concentration are tested on the plume images. A validation is done on the gas plume model using experimental data collected on a SF_6 plume. Results show the integrated plume model to be in good agreement with the actual data from five to one hundred meters from the stack exit. The validity and limitations of these models are discussed as a result of these tests. [S0091-3286(00)01804-3]

Subject terms: remote sensing; hyperspectral; gas plumes; synthetic image generation.

Paper 980483 received Dec. 30, 1998; revised manuscript received Sep. 21, 1999; accepted for publication Oct. 8, 1999.

1 Introduction

Remote sensing of factory stack plumes using hyperspectral sensors has the potential to reveal information about the constituents of the plumes. The makeup of the plume, such as the species type and its temperature and concentration, can help regulatory agencies monitor factory emission products and their rate of release into the atmosphere. This can be done either with ground based hyperspectral sensors looking up through the plume, or airborne sensors looking down. Both passive and active remote sensing of plumes are currently being investigated. While active methods (i.e., laser remote sensing) can provide more accurate determination of the concentration of effluents in the plume, they can only provide information at certain wavelengths. In addition, active platforms have limited coverage and are expensive to produce and maintain. Passive sensors on existing platforms can provide information on plumes over a wide spectral band, and image fusion can be used to yield additional information. Coverage also would be more widespread and reliable.

Synthetic image generation (SIG) will aid in the investigation of plume phenomenology and in the understanding of remote sensing of plumes. SIG is the process of using first principles from radiometry to simulate an image as seen by a particular sensor. SIG provides the ability to model images under a variety of conditions (wavelength, sensor platform, scene conditions, etc.). These synthetic images can then be used to predict sensor performance under various conditions, and provide a way to test remote sensing algorithms. Synthetic plume imagery can reveal not only how a plume will look to a sensor, but also how it will interact with the background and surrounding atmosphere. A variety of plume images can be generated using different sources, meteorological conditions, viewing conditions, and wavelengths. Algorithms designed to determine effluent concentration can be tested on these images to determine their accuracy and robustness.

The radiance reaching the sensor from the plume originates from several sources. Direct sunlight and diffuse skylight are scattered from the plume. The type of scattering (Mie or Rayleigh) depends on the spectral band and particulate size. The intensity of scattering depends on the concentrations and particle size distribution. Thermal self-emission and absorption by the plume will be apparent in the MWIR (3–5 μm) and LWIR (8–12 μm) regions. The amount of self-emission depends on the emissivity and temperature of the plume. The transmission will be dependent on the spectral absorbance of the plume constituents.

The generation of synthetic images of plumes must account for all of these factors to produce a radiometrically accurate image. The Digital Imaging and Remote Sensing Image Generation code (DIRSIG) was developed for this purpose.[1] It is currently employed by the Center for Imag-

ing Science at the Rochester Institute of Technology for simulating images for various remote sensing platforms. DIRSIG is a ray-tracing code that incorporates MODTRAN to produce a radiometrically accurate image at the sensor of a scene built by the user.

In this article we discuss the research and results in developing a radiometrically accurate method for producing synthetic images of plumes. The methods need to account for the main interactions of the plume with its environment. Existing plume models for factory stack plumes are used to provide the plume geometry and characteristics (constituents, concentration, and temperature). The effects of self-emission and absorption from the plume are incorporated in DIRSIG on a pixel-by-pixel basis. Atmospheric effects are accounted for using MODTRAN. Different spectral gas databases are included in order to model a variety of gas plumes.

A validation is also done on the models developed in this research. The results of the DIRSIG gas plume model are compared to the experimental data collected of a SF_6 plume at the Nevada Test Site.

A specific example is given on how the plume model can aid hyperspectral imaging sensors in the detection of gas plumes. A simulation of a trichloro-ethanol plume is done and the signals at various distances downwind of the stack exit are examined. Sensitivity studies are done on the plume-background contrast based on changes in the plume characteristics. Finally, a plume image is made with varying meteorological conditions, illustrating a plume that wanders and puffs.

2 Factory Stack Plumes

Release of various chemical effluents by a factory into the atmosphere can reveal materials that are being used or produced by the factory. Common emissions from power plants include CO, CO_2, NO, NO_2, N_2O, SO_2, HCl, CH_4, NH_3, H_2O, and NCHO. Sulfur hexafluoride (SF_6) is commonly used as a plume tracer gas due to its large absorbance cross-section. These particulates typically have[2] diameters under 0.1 μm. The exception is NO_2 which can have diameters around 0.6 μm and is the dominant absorber in the visible region.[3] The local humidity level can cause an increase in particulate size due to condensation of water vapor onto the nuclei.[4] Normally, there is very little scattering unless flyash and sulfates are present in large amounts (which may occur in modern fossil fuel power plants not under emission control). A comprehensive study of factory stack emissions, including computer code to simulate them, was done[5] by the EPA between 1979 and 1981.

The chemistry within the plume can be very complex. Some gases that emerge from the stack are converted to particulates as they interact with the atmosphere. For example sulfur dioxide will change into sulfate, and nitrogen dioxide to nitrate. The rate of conversion depends strongly on the atmospheric conditions. The temperature of the plume also drops as the cooler ambient air is entrained into it. The rate of entrainment depends on the turbulence and location of the boundary layer of the lower atmosphere. All of these effects increase the difficulty of accurately modeling the mixture of gases and particulates and their concentration downstream of the stack.

From an imaging perspective, the amount of sunlight scattered from a factory plume towards the sensor will depend on the type of particulate, its concentration, and its size distribution function. Most gas plumes scatter weakly due to the small particulate size. The type of scattering will generally be of the Rayleigh type. If sufficient concentrations of water droplets are present in the plume, they will be the dominant source of scattering. An exception is when sulfates and flyash are present in the plume. These particles have diameters of 0.5 μm and larger and cause Mie scattering of visible light.

The detection and quantification of gases in the plume by remote sensing present some unique problems. Many variables are involved in the formation of the plume that make the inverse problem of characterization difficult. Both active (LIDAR) and passive techniques have been investigated and developed. One of the most successful methods uses Fourier Transform Infrared Spectroscopy (FTIR). Much work has been done in this area of detection and quantification of molecules in plumes.[6] Signal processing techniques are used to match the spectrum with known gas signatures that may exist in the plume. A plume analysis code was written for FTIR sensors and used to determine contrast SNR for a sensor on an airborne platform against different temperature plumes.[7] The types of gases, and their mixing ratios, can then be used to determine the products of the factory. While FTIR can provide spectral data, it does not provide any spatial data. However with the new generation of hyperspectral imaging sensors, the potential now exists to extract both spectral and spatial information from remotely sensed images of the plume. Spatial information would help give the physical dimension of the plume as well as provide mixing ratios of the gases as a function of position within the plume. In addition simultaneous measurements of background signature can be used to improve the SNR of the plume signature. Work is currently being done with the Thermal Infrared Imaging Spectrometer (TIRIS) for plume detection.[8] This is a pushbroom system which operates from 7.5–14.0 μm in 64 spectral bands. Spectral resolution is 10 cm^{-1} at 10 μm.

3 Theory

3.1 *Plume Modeling*

Modeling plumes is a very complex process that involves hydrodynamic and turbulence flow theory. The aim of this research was to model the images of plumes and not the plumes themselves, thus only a brief description of plume modeling will be given.

The plume model used in DIRSIG is designed to model gas plumes released from a factory stack. It was originally developed by the EPA,[9] and has been modified by Kaman Corporation and the Jet Propulsion Lab (henceforth called the JPL model). It is currently being maintained by RSA Systems. The JPL model is a Gaussian plume model based on the Brigg's equation for plume dynamics. For a neutral atmosphere, the Brigg equation is commonly used to give the plume centerline height. It assumes a buoyant rise of the plume. The plume entrains ambient air at a rate proportional to its velocity and cross-sectional area relative to the surrounding area. For a neutrally buoyant effluent, the plume height is:

$$h = h_o + 3\left(\frac{r_o m^2}{m+3}\right)^{2/3} x^{1/3}, \tag{1}$$

where h_o is the stack height, r_o is the stack radius, x the downwind distance, and m the emission velocity ratio, defined as the vertical emission velocity divided by the wind velocity. A Gaussian distribution of the concentration of gases or aerosols from the plume centerline is assumed of the form:

$$C = \frac{Q}{2\pi\sigma_y\sigma_z\mu}\exp\left(-\frac{y^2}{2\sigma_y^2}\right) \times\left[\exp\left(-\frac{(z-h)^2}{2\sigma_z^2}\right)+\exp\left(-\frac{(z+h)^2}{2\sigma_z^2}\right)\right], \tag{2}$$

where y is the lateral distance from the centerline, z is the vertical distance from the ground, Q the source intensity (mass released per unit time), μ is the mean wind speed, h the plume centerline (from the Brigg's equation), and σ_y (or σ_z) is the lateral (or vertical) coefficient of dispersion. The values for σ_y or σ_z decay as the downwind distance increases, with the decay rate being derived by fitting curves to empirical measurements.[10]

The dilution factor at a particular position within the plume can be found by dividing the original stack concentration $C_o = Q/\pi r_o^2 w$ by C:

$$D = \frac{Q}{C\pi r_o^2 w} = \frac{2\sigma_y\sigma_z}{r_o^2 m}\exp\left(-\frac{y^2}{2\sigma_y^2}\right) \times\left[\exp\left(-\frac{(z-h)^2}{2\sigma_z^2}\right)+\exp\left(-\frac{(z+h)^2}{2\sigma_z^2}\right)\right], \tag{3}$$

where w is the vertical emission velocity and $m = w/\mu$. It should be noted that the Gaussian model in the lateral direction holds for all stability conditions, while the vertical distribution only holds for stable and neutral atmospheric conditions.

The JPL model calculates the initial conditions at the stack exit for several parameters including plume temperature and VMR. The dilution factor is then calculated downwind at any point within the plume using Eq. (3). The parameters of the plume at that point are then determined by multiplying the dilution factors with the initial parameters at the stack exit. The JPL model is designed for factory stack plumes containing multiple species. Inputs to the code include gas type and release rate, stack geometry, and meteorological conditions (including time-varying conditions). The outputs are downwind location, plume centerline height, and plume characteristics (dilution, temperature, and volume mixing ratio (VMR)).

3.2 *Gas Absorption*

The different species in a gas plume absorb light at various wavelengths, depending on the electronic, vibrational, and rotational bands. The field of spectroscopy specifically considers how gases can be identified by their absorption ''fingerprints.'' Since modeling of gas plumes requires knowledge of the absorption spectrum, this section will briefly touch on this process. There are several texts that give a more complete coverage of this topic and how it relates to remote sensing.[11–13]

The actual absorption line shape is determined by several factors. The first is natural broadening which results in a band of transition levels due to quantum mechanical effects. This is a minor factor in gas plumes since frequent collisions between molecules shorten the natural lifetime in the excited state. These collisions contribute to pressure broadening of the line shape. The resulting shape is described by a Lorentzian function and the half-width is determined by the atmospheric pressure and temperature. The Doppler effect also broadens the absorption line. This profile is described by a Maxwellian distribution and again depends on atmospheric pressure and temperature. The importance of pressure vs. Doppler broadening is expressed as a ratio,

$$\frac{\alpha_D}{\alpha_L} \approx 10^{-12}\frac{\nu_o}{p}, \tag{4}$$

where α_D and α_L are the half-widths of the Doppler and Lorentzian profiles, ν_o is the center frequency (in Hz), and p is the pressure in mbars. In the LWIR at 10 μm at a pressure of 1000 mbars, this ratio is 0.03 indicating that pressure broadening is the main factor in determining line shape.

The absorption coefficient $k_{\text{abs}}(\nu)$ is defined as,

$$k_{\text{abs}}(\nu) = S \cdot f(\nu - \nu_o)[\text{m}^{-1}], \tag{5}$$

where S is the strength factor of the absorbing line (based on the transition probability) and f is the line shape function centered on ν_o. The transmission through a gas plume is found using the Beer-Lambert law (also known as the Bouguer law)

$$dE = k_{\text{ext}} E\, dz \quad [\text{W/m}^2], \tag{6}$$

where E is the irradiance, k_{ext} is the extinction coefficient, and dz a unit path length (the implicit dependence on wavelength has been omitted). When scattering is negligible (as in the case of gas plumes), then the extinction and scattering coefficient are the same. The exponential form for a homogeneous medium is

$$E = E_o e^{-k_{\text{ext}}x} \quad [\text{W/m}^2]. \tag{7}$$

The term $k_{\text{ext}}z$ is referred to as the optical thickness or optical depth, τ'. The transmission is the ratio of irradiance out to irradiance in:

$$\tau = \frac{E}{E_o} = \exp(-k_{\text{ext}}z) = \exp(-\tau'). \tag{8}$$

For a plume with multiple constituents, the transmission is expressed as

$$\tau = \exp\left(-\sum_i k_{\text{ext}_i} z\right), \tag{9}$$

where the individual extinction coefficients for each constituent are now summed together. Databases for gases often measure transmittance in terms of absorbance

$$A = -\log_{10}\tau. \tag{10}$$

The absorbance is measured for a gas at a particular temperature and column density. The column density is the VMR of the gas multiplied by the path length of the gas and is expressed as ppm-m.

For a plume with a known VMR and temperature, k_{abs} is derived from the absorbance of a given database through

$$k_{\text{abs}} = \frac{A_{DB} \cdot \text{VMR}_P \cdot T_P}{\log_{10}(e) \cdot CD_{DB} \cdot T_{DB}}, \tag{11}$$

where A_{DB}, CD_{DB}, and T_{DB} are the absorbance, column density, and temperature from the gas database and VMR_P and T_P are the volume mixing ratio and temperature of the particular gas species in the plume. If there are multiple gas species, then the total absorption coefficient of the plume is the sum of the individual coefficients. If the column density of the plume is given, then the optical depth of the plume can be found from:

$$\tau' = \frac{CD_P \cdot T_P \cdot A_{DB}}{\log_{10}(e) \cdot CD_{DB} \cdot T_{DB}}, \tag{12}$$

where CD_P is the column density of the plume.

3.3 *Gas Thermal Self Emission*

In addition to absorption of photons, the plume will also emit radiation by thermal self-emission. For a perfect Lambertian blackbody, the spectral radiance is described by Planck's equation

$$L_{\lambda BB}(T) = \frac{2hc^2}{\lambda^5(e^{-hc/K\lambda T} - 1)} [\text{Wm}^{-2}\text{sr}^{-1}\text{um}^{-1}], \tag{13}$$

where h, c, K, and T are Planck's constant, the speed of light, Boltzmann's constant, and the temperature in degrees Kelvin, respectively. The emissivity of an object is a measure of how well it radiates compared to a perfect blackbody:

$$\varepsilon(\lambda) = \frac{L_\lambda(T)}{L_{\lambda BB}(T)}. \tag{14}$$

Following Kirchoff's law (that a perfect particle emits all it absorbs), the emissivity can be defined as

$$\varepsilon = \alpha = 1 - e^{-k_{\text{abs}}z}, \tag{15}$$

where α is the absorption of the medium. The assumption here is that the particle is in local thermodynamic equilibrium. The model for plume self-emission is based on Kirchoff's law and thus the self-emitted radiance depends on the absorption coefficient. This means that the plume strongly absorbs (low transmission) at the same wavelengths where it strongly emits. If all transmission losses are due to scattering, then there is no self-emission.

3.4 *Governing Equations for Remote Sensing*

For the case of gas plumes where the particulates are small and the solar radiation is small compared to thermal self-emission (MWIR and LWIR wavelengths), scattering will be considered negligible and not accounted for. Consider a ground-based sensor looking up through a plume.

In the LWIR where self-emission is dominant and scattering is negligible, the radiance reaching the sensor is:

$$L = \varepsilon_P L_{PBB} + L_{D\varepsilon}(\phi, \theta)\tau_P [\text{Wm}^{-2}\text{sr}^{-1}]. \tag{16}$$

The first term is the plume self-emission and the second term is angular downwelled atmospheric self-emission as a function of the azimuth and zenith look angle. The plume transmission is based on the Beer-Lambert Law where attenuation is due solely to absorption and $\varepsilon = 1 - \tau$. Any effects from the atmosphere under the plume are ignored. Thus no transmission losses or self-emission is accounted for from this region.

An airborne sensor looking down will have additional radiance sources from the intervening atmosphere. In the LWIR, the radiance is:

$$L = (1 - r_E)L_{E\varepsilon}\tau_P\tau_{\text{atm}} + \varepsilon_P L_{PBB}\tau_{\text{atm}} + L_{D\varepsilon}r_{\text{dif}}\tau_{\text{atm}} + L_{U\varepsilon}[\text{Wm}^{-2}\text{sr}^{-1}]. \tag{17}$$

The first term is the earth's thermal self emission, the second is the plume's self-emission, the third is the downwelled atmospheric self-emission diffusely scattered by the plume, and the last term is the upwelled radiance from the atmosphere. Again the atmosphere under the plume is considered negligible. Also the reflection of the plume off the background is considered negligible.

4 DIRSIG Plume Model

The governing equations just described are utilized by DIRSIG to construct a plume image for a scene as viewed by a particular sensor. A comprehensive discussion of DIRSIG can be found in the referenced report.[1] Only some highlights of DIRSIG will be covered here.

The synthetic scene is constructed using Automated Computer Aided Design (ACAD) to produce wire-frame objects (not including the plume). Faceted elements are assigned material attributes that contain optical and thermal properties. The ACAD scene is used with a ray tracer model. A sensor location is defined within the geometry. A ray is traced into the scene from each pixel in the sensor. In this way, the sensor-ground instantaneous field-of-view (GIFOV) is overlaid on the scene. When a facet is encountered within a pixel GIFOV, several calculations are made. The first determines the thermal self-emission from the facet that would be transmitted back to the sensor. Then, if the target is diffuse (Lambertian assumption), the radiance reflected from that facet due to downwelled skylight and atmospheric emission is determined. For specular facets, the ray is reflected to determine whether the sun, sky, or another background object is hit. Atmospheric transmission, self-emission, and scattered sunlight are determined through MODTRAN. A radiance database is generated before the DIRSIG run. The database is then accessed for

Table 1 Input parameters for plume model

Plume adjustment	Plume initial conditions	Scene meteorological	Scene geometry
dilution minimum	species type	wind direction (deg)	stack height (m)
dilution change	release rate (lbs/hr)	wind speed (knots)	stack diameter (m)
sampling step size	plume release temp. (F°)	atm. stability number	stack location (m)
contrast contribution	release velocity (m/s)		target point (m)
number planes modeled			sensor point (m)
sampling time interval			

each ray-trace to determine values like transmission and atmospheric path radiance along the sensor to facet path.

The plume model is integrated directly into DIRSIG and is run for each ray-trace in the scene. The user determines the effluents contained in the plume, and multiple effluents are possible. Numerous parameters are used to determine the characteristics of the plume. They can be grouped into four categories: (1) plume adjustment parameters, (2) plume characteristic parameters, (3) scene meteorological parameters, and (4) scene geometry parameters. Table 1 shows the parameters in each category.

The ''plume adjustment'' parameters govern the shape and characteristics of the plume. For example, decreasing the ''dilution change'' parameter will increase the dilution factor. Increasing the number of plume planes will increase the length of the plume downwind. The sampling step size is given as a fraction of the stack diameter. These parameters can be adjusted so as to match the plume model with any available experimental data.

The ''plume initial conditions'' parameters determine the initial conditions of the plumes. Up to ten species type and their individual release rates can be specified. The molecular weight of each species is also needed. The release rate, release velocity, and stack diameter will impact the downwind VMR and column density.

The ''scene meteorological'' parameters determine the meteorological conditions at the stack. This can be described either through time-varying conditions or as a time-averaged condition. If the time-averaged parameters are used, a plume with constant shape results. If time-varying conditions are used by specifying a meteorological file, then the user must supply the parameters as they vary over time. By using time-varying parameters, the plume can be given some texture and made to ''puff.'' The wind speed controls how much the plume is bent over. The atmospheric stability number determines how quickly the plume disperses; the lower the number the lower the dilution downwind. In the current version, these plume parameters do not interact with the MODTRAN generated atmosphere, and care must be taken that the meteorological conditions are consistent for both models.

The constituents of the plumes are determined from a gas absorbance database taken from the combined USAF/EPA Internet web site. This site contains both experimentally measured databases as well as HITRAN generated databases for several gases. It gives the gas absorbance as a function of frequency (at 0.25 cm^{-1} intervals) for a given column density and temperature. Most of the gas databases have a frequency range from 600 to 4500 cm^{-1} (2.2 $-16.6\,\mu$m). The smeared-line model is used to interpolate up from the database resolution to the spectral resolution of the hyperspectral sensor. This assumption is valid only if the spacing between the spectral lines is less than the linewidths themselves.[14] While this may not be the case for all gases, this assumption is used. This may result in an underestimation of the absorption if the spectral lines do not overlap. The smeared-line model also holds if the concentration is weak enough so that the optical depth is less than one.

For every ray-trace in the scene, the JPL model is called. The location of the sensor and the target hit point are recorded and passed to the JPL model. If the trace is to the sky, the product of the direction vector and a large distance determines the target point. The JPL model then determines if the plume is hit by the ray based on the input parameters. A bounding volume check for the plume is made for the ray to save compute time. If it is determined that the ray intersects the plumes, then the column density and temperature along that ray are calculated. The column density is found by integrating the VMR for each distance increment along the ray. The temperature is the average along the ray. The column density and temperature, along with the number of species present, are returned to DIRSIG.

DIRSIG checks to see if the returned temperature is greater than zero. If so, the plume is present for that ray-trace. The ratio of the returned column density and temperature to the corresponding database values is used to determine the optical depth through Eq. (12). If there are more than one species, then the individual optical depths are summed together. The Beer-Lambert Law is used to determine the transmission through the plume at that point. The emissivity is taken as one minus the transmission, and the plume self-emission is the emissivity times the Planck blackbody radiance at the plume temperature. The self-emitted radiance and plume transmissions are then used with the background and atmospheric calculations in Eq. (16) or (17) to determine the total radiance reaching an upward or downward (respectively) looking sensor.

5 Validation

The DIRSIG plume model was validated against data collected on a SF_6 plume released at the Nevada Test Site (NTS). A comparison of the plume characteristics, radiance values, and plume-background contrast is made at the peak absorbance spectra for the gas (10.5–10.75 μm). Because the validation is in the LWIR region, only absorption and self-emission effects are taken into account. Note that all radiance values here are integrated over the appropriate spectral band and given in μ Watts-cm^{-2}-sr^{-1}.

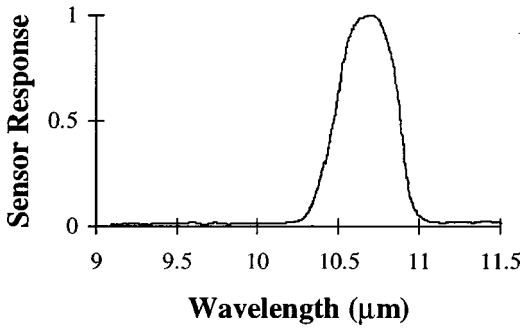

Fig. 1 Sensor response of the TI IRLS-RS18c sensor.

In February and March of 1994 the Effluent Tracking Experiment was conducted at the NTS. A variety of chemicals were released to simulate a chemical manufacturing site. A particular data set from 25 February was chosen for use in the validation. Vaporized SF_6 was mixed with hot air from a jet start cart and released from a 71-foot tall stack with a 0.413 m diameter. SF_6 is an inert gas with a strong absorption and emission band from 10.5 to 10.75 μm. A description of the chemical release parameters can be found in the referenced report.[15]

The sensor used for the data collection was a Texas Instrument IRLS-RS18c multi-spectrometer. There were 6 bands ranging from 7.75 to 11.75 μm. The band chosen for the validation data is from 10.4 to 11 μm. Figure 1 shows the spectral response of the sensor at this band.

This band is tuned to the peak absorbance curve of SF_6. At this band a 400 by 400 pixel image of the plume was collected with calibrated radiance values. The image from the sensor is shown in Fig. 2. The scene contains reflectance cards as well as a string of distance markers. These markers are spaced 25, 50, 100, and 200 meters apart. The plume is seen distinctly the first 25 m from the release point, and then fades away quickly. The plume passes over a bright patch of ground and ''disappears'' due to the lack of contrast. The bright patch is most likely due to a change

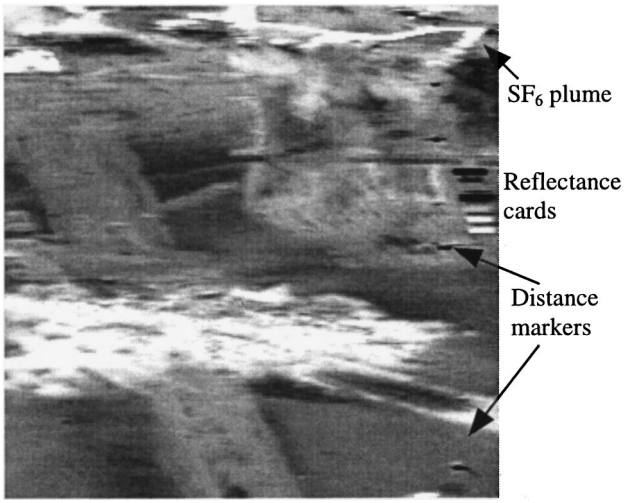

Fig. 2 SF_6 plume images of TI ILRS-RS18c.

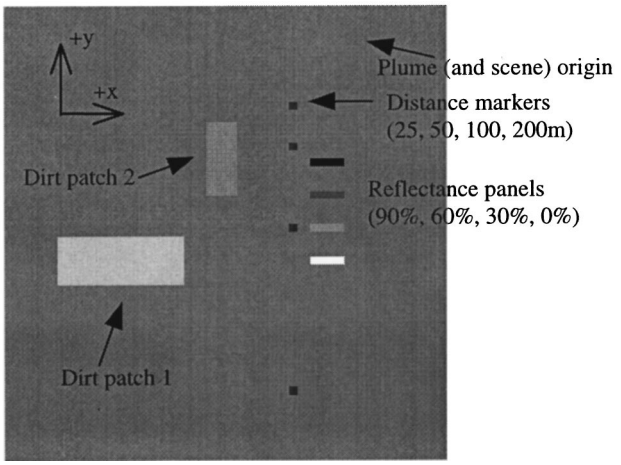

Fig. 3 DIRSIG scene of NTS background.

in emissivity from the surrounding ground. It then reappears for a short distance before passing over an even brighter patch of ground.

The images were taken at 4:18 P.M. The ambient air temperature is at 18.5 C° with an average ground temperature of 9 C° and a wind speed of 3.4 m/s (~7 knots). These support data were collected later in the afternoon at 5:20 P.M. The sensor is at an altitude of 152 m with a ground speed of 100 knots. The release rate of SF_6 is 50 lbs/hr at a temperature of 363 K°. The stack release velocity is 15 m/s.

The first step in creating the DIRSIG scene is to create the background. The main objects in the scene are the background, the first bright patch the plume passes over (labeled dirt patch 2), the second brighter patch (labeled dirt patch 1), the distance markers, and 4 reflectance panels. The temperature of all these objects are set to the average measured temperature of 9 C°. No experimental information was provided on the emissivities of the dirt and the patches. The emissivities of these objects in DIRSIG (except for the reflectance panels) are calibrated so as to match the measured radiance. The background and dirt patches are intended to represent the average radiance in that area (based on the measured radiance). The reflectance panels have reflectances of 90%, 60%, 30%, and 0%. The markers have a 70% reflectance. An overhead scene of the ACAD model is shown in Fig. 3.

Since the exact coordinates of where the sensor was are unknown, the view angles for the scene are set-up to best recreate the scale and angle of the actual scene. The plume release point is set to an absolute coordinate value of $(x,y,z)=(0,0,0)$. The scene center is located at $(-80, -40, 0)$, with units in meters, and the sensor is located at $(-80, -354, 350)$. The sensor has a 50 mm focal length and is looking down 30° below the horizon. Note that the reported sensor altitude is lower (~152 m), but the correct look angles could not be reproduced using that altitude.

The same frequency bands and the appropriate sensor response are recreated in DIRSIG. The band has a frequency from 910 to 960 cm^{-1} at a 5 cm^{-1} interval (10.4167–10.989 μm). MODTRAN is used to calculate the appropriate atmospheric transmission and upwelled. The sensor response is taken from Fig. 1. Figure 4 shows a side view of the DIRSIG plume model.

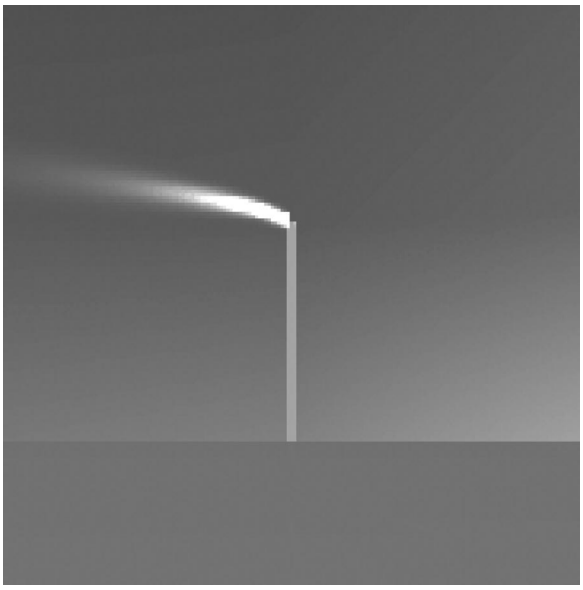

Fig. 4 Side view of DIRSIG plume model.

The total computer run time for this image is approximately fifty minutes using a DEC Alpha workstation. The plume extends out to approximately 225 m, however it is only visible for the first 100 m. The plume has a Gaussian shape out to about 100 m, and beyond that remains constant. This is because the plume code is set to register the presence of a plume only when the column density is greater than 1 ppm-m. Thus the plume actually shrinks further downwind because of this condition. The temperature profile along the centerline of the plume is derived using the plume debug images. This can be compared with the actual measured plume temperature during the experiment (although the temperature was not measured at exactly the same time as the image was taken). This temperature was derived using a blackbody fit based on measurements from a spectrometer. This is plotted in Fig. 5.

DIRISIG over predicts the plume temperature for the first 15 m. At 10 m the DIRSIG temperature is approximately 10% higher than the measured temperature. This error may be expected since entrainment of ambient air is not modeled and thus the plume does not cool off as quickly. However further downwind the model and experimental data match quite closely (less than 10%) when the difference in ambient temperature is accounted for. The column density profile along the centerline can also be plotted using the debug images. This is shown in Fig. 6.

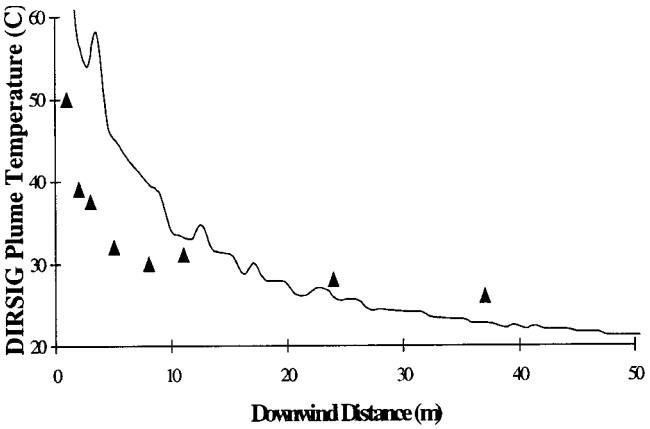

Fig. 5 Measured (▲) and DIRSIG (—) plume temperature downwind from stack.

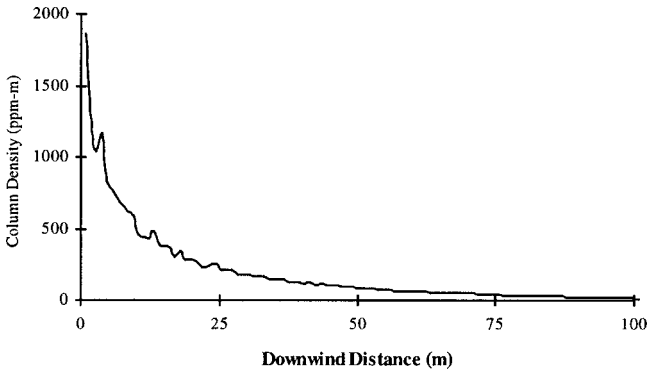

Fig. 6 DIRSIG column density downwind from stack.

The same trend as the plume temperature is evident with a rapid drop-off in value in the first 25–30 m and then a gradual leveling out. This is because in the model both the temperature and VMR are based on a common dilution factor. No experimental data were available showing the column density as a function of downwind distance. However, the Aerospace Ram Van spectrometer did take profile measurements of the column density across the plume at certain downwind distances. One particular measurement was taken 100 m downwind. The Ram Van and DIRSIG profiles are shown in Fig. 7.

The peak column densities of both measurements are in good agreement with an error of less than 5%. The profile of the DIRSIG plume is wider by about 5 m, or 20%, than the measured profile. This is caused by a variety of conditions, most notably the difference in the instantaneous atmospheric conditions that are set in the plume model. The only other column density profile available is at 500 m, which is beyond the downwind distance of the DIRSIG plume model.

The scene is then run using the NTS look angles. Figure 8 shows the image. The plume is easily visible for the first 30 m, and then starts to fade rapidly. The plume is barely

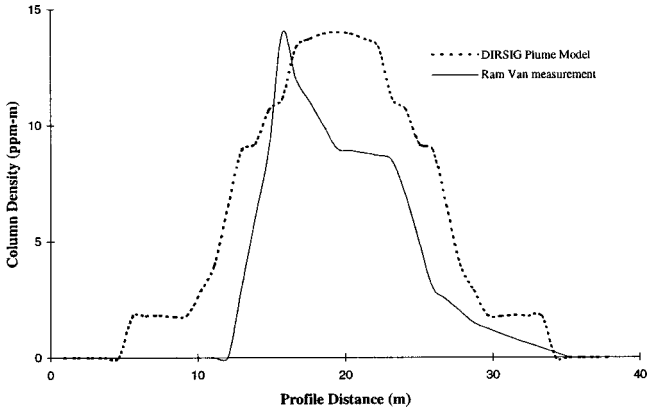

Fig. 7 Column density profile at 100 m downwind of stack.

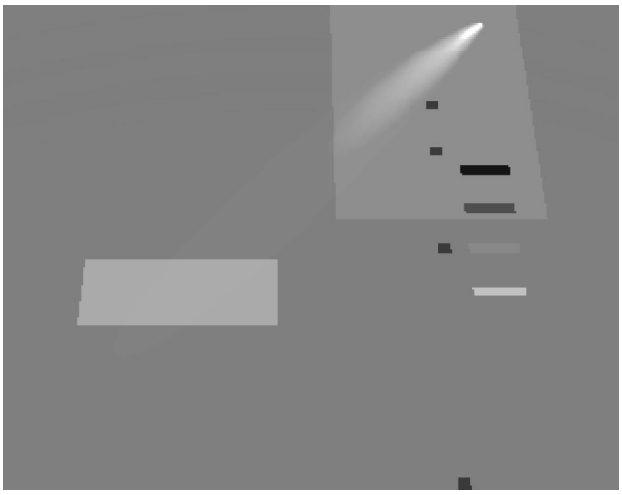

Fig. 8 DIRSIG plume model using NTS look angles.

visible over the background, and loses contrast over dirt patch 1. The radiance profile (in μWatts/cm^2/sr) along the centerline of the plume is taken for the first 35 m and shown in Fig. 9.

There is significant overestimation by DIRSIG in the first 5 m. This is the same case as with the plume temperature (possibly due to inaccurate entrainment modeling). After that, the gap between the two profiles narrows to where DIRSIG overestimates the radiance by about 20%. The bumps in the NTS images are from the variation in the background, which is uniform in the DIRSIG image. Remember the radiance value from the DIRSIG background is set to match that from the NTS images, thus effectively eliminating any bias in the plume radiance value. Cross-sectional radiance profiles across the plume were taken at 7 m and 100 m downwind. The results at 7 m are shown in Fig. 10.

As expected the peak radiance of the DIRSIG model is 40% higher than in the NTS data. However, the profile width matches fairly close, indicating the spatial extent of the DIRSIG model is correct. The profiles 100 m downwind are shown in Fig. 11. At 100 m downwind the DIRSIG values are now lower than the NTS plume, with the error in the peak values now less than 15%. This corresponds to the good agreement in the column density measurements at 100 m (see Fig. 6).

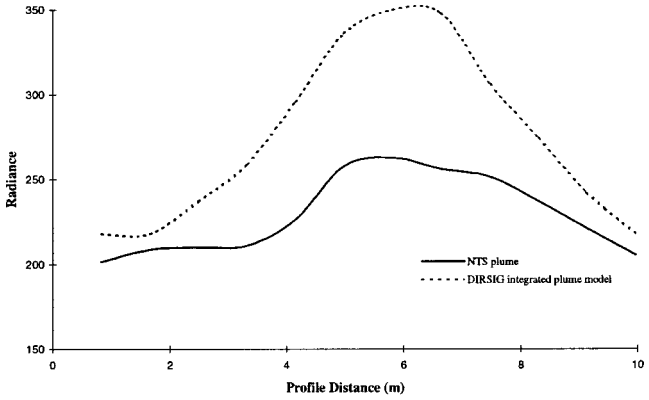

Fig. 10 Cross-sectional radiance profile of plume 7 m downwind.

From these comparisons with the NTS data, some observations about the validity of the DIRSIG plume model can be made. In the first 5 m the DIRSIG plume significantly overestimates the radiance value. This may be associated with the difficulty in modeling the turbulent jet-like flow coming right out of the stack. It seems entrainment of the ambient air is not quick enough, and the dilution factor remains too high in the model. After this point the model and data come into fairly good agreement. The profile at 100 m shows an error less than 10%. However, after 100 m the DIRSIG plume starts to dissipate faster than the NTS plume, as evident in the image. This is in part due to the plume model, which cuts off the plume if it falls below 1 ppm-m. Also at these distances from the stack, the variability in meteorological conditions has had more time to impact the formation of the plume. The DIRSIG plume is run with constant meteorological conditions. It can be summarized from these validation results that the integrated DIRSIG plume model overestimates the plume radiance under 5 m from the stack, is in agreement to within 20% from 5 to 100 m, and then underestimates the radiance beyond 100 m due to limitations in the JPL plume model.

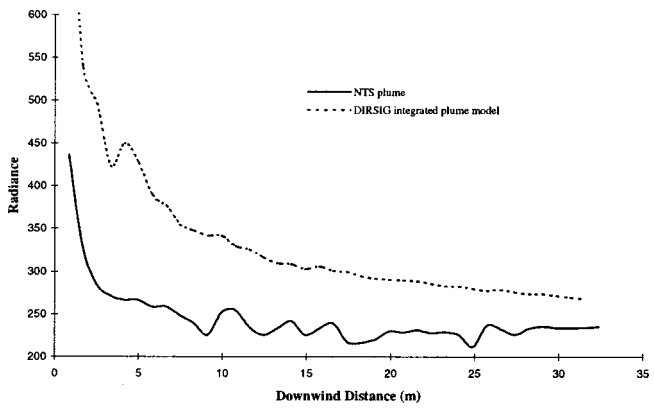

Fig. 9 Downwind radiance profile.

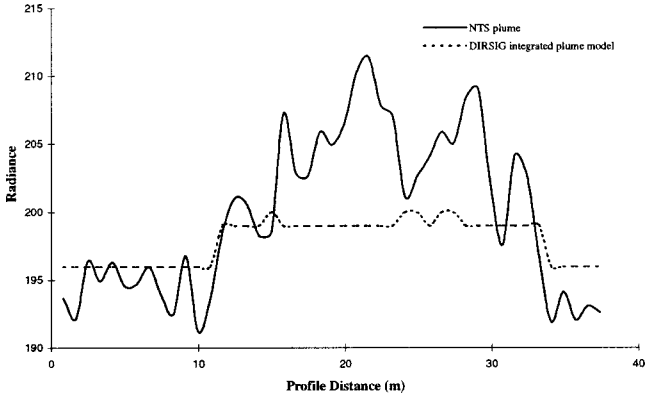

Fig. 11 Cross-sectional radiance profile of plume 100 Meters downwind.

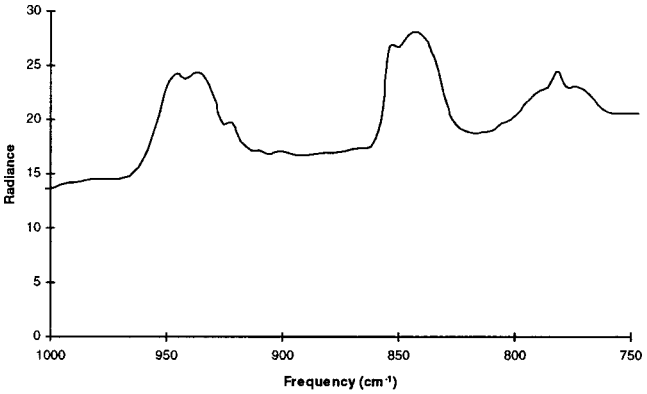

Fig. 12 Scene radiance at stack exit.

6 Applications of the Model

This final section demonstrates an application for this modeling tool. With the advent of hyperspectral imaging, it is possible to determine the plume signal at multiple points downwind of the stack from a single image. Of interest is how far downwind useful information about the plume can still be determined. This information may be species type or concentration. With the DIRSIG plume model, analysis can be done by sampling pixels in the synthetic image and examining spectral signal.

A trichloro-ethanol (C_2HCl_3) plume was modeled. The parameters were identical to the NTS plume. The background was composed entirely of grass. A hyperspectral sensor from 10–13.7 μm with a spectral resolution of 4 cm^{-1} with unity response across the band was used. The sensor was located at an altitude of 1 km.

The simulated image looks similar to Fig. 4. The spectral signature (68 bands) was sampled along the downwind axis of the plume. These points were taken at the stack exit, 5, 10, 20, 40, 50, and 75 m downwind. The radiometric signal recorded at the sensor includes not only the plume signal, but also the grass background and intervening atmosphere. A plot of the spectral radiance at the stack exit is shown in Fig. 12.

The blackbody temperature curve of the grass (300 K) can be seen with the absorption peaks of the gas sticking out. A simple background subtraction can be done by taking a non-plume pixel and subtracting it out from the plume pixel. When this is done the more familiar spectral signature of the gas can be seen. This simple background subtraction was done for the 7 spatial points downwind, and plotted in Fig. 13.

As can be seen, the signal drops off quickly beyond 40–50 m downwind. The ratio of the signal at 5 m is 31 times stronger than at 75 m for the absorption curve at 842 cm^{-1}. The ratio between the peaks also changes from the laboratory absorbance data. The lab data show a ratio of the middle to left to right peak of about 10:8:2. After incorporating the background and atmosphere into the signal, the ratio (at the exit) is about 10:9.5:4. Further downwind (50 m) the ratio is 12:10:3.6. The spectral resolution is a main factor in determining how much this ratio is smoothed out. Note that negative radiances are possible when using the background subtraction. This case would occur when the plume temperature is the same as ambient, but the concentration is still strong enough to partially block out the background.

These ''cold'' plumes absorb more of the radiation than they emit. The information from this simulation can be used for several applications. One of them is species identification. Algorithms can be tested to determine how far downwind a species might be identified from a stack. The robustness of the algorithm will be dependent on the stack release rate, release temperature, and atmospheric conditions, all of which are parameters that can be varied in the model. Also inverse algorithms can be tested. These are algorithms that try to determine the gas concentration based on the signal at the sensor. Again, the success of these algorithms is strongly dependent on the parameters mentioned above. The authors have tested one of these algorithms[16] and its robustness to plume temperature. These results will be reported in a future paper.

The DIRSIG plume model can also be run with varying meteorological conditions to generate a more realistic looking plume that puffs and wanders. This may be useful in

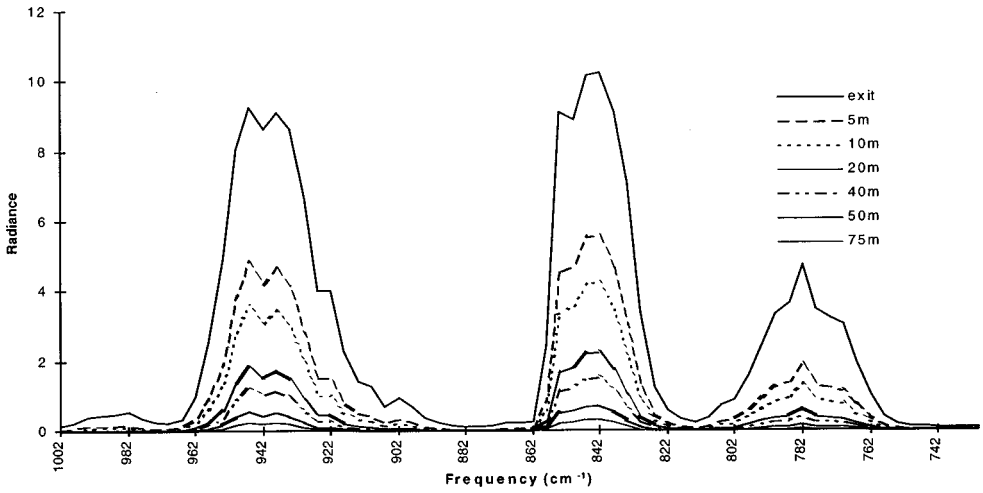

Fig. 13 Comparison of radiance downwind along plume axis.

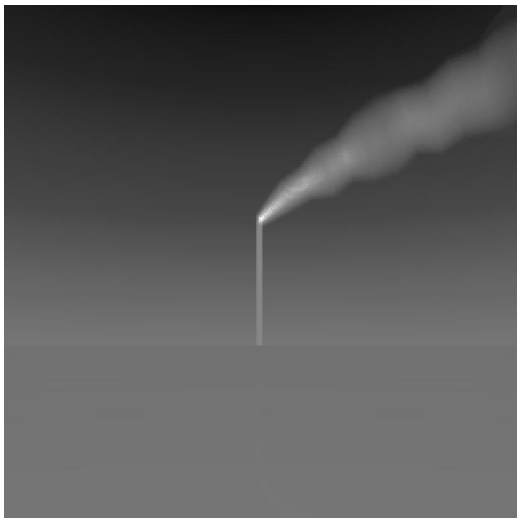

Fig. 14 Side image of wandering and puffing plume.

another application such as mission planning for a plume release field experiment. Running the plume model would help determine the optimal positioning of the hyperspectral sensor, as well as other instrumentation. A simulation was run where the wind velocity, direction, and atmospheric conditions were varied over five second intervals. The resulting side image is shown in Fig. 14.

7 Conclusions

A method to generate synthetic images of plumes using DIRSIG has been presented. An existing model of plume dynamics is used to determine the shape and characteristics of the plume in the image. DIRSIG computes the radiometric signal from both the plume and background by performing a ray-trace on a pixel by pixel basis. The JPL plume model is directly called within DIRSIG to produce an integrated plume in the scene. In addition to producing the radiometric image, several images of other plume characteristics (transmission, temperature, etc.) can be generated.

Attempting to account for all the physical interactions that occur between the plume and its environment is an ambitious task. The work done here is a first-cut attempt at trying to simulate the main interactions. One of the limitations to the accuracy and validity of the DIRSIG plumes is the model of the plume itself. If the plume model does not accurately predict the plume characteristics, then the plume images will not be accurate. The adage of ''garbage in garbage out'' applies here.

The validation of the JPL model is done against data collected for a SF_6 plume. The model overestimates the radiance by a factor of two within the first 5 m of the stack, and then is within 20% of the actual values out until 100 m. The downwind radiance and column density cross-sectional profiles at 100 m have errors less than 15%. For distances greater than 100 m downwind, the model underestimates the radiance. This is due to the difficulties in accurately modeling a plume at far distances from the stack.

References

1. J. Schott, *Remote Sensing: The Image Chain Approach*, Oxford University Press (1996).
2. D. L. Blumenthal et al., ''Effects of a coal fired power plant and other sources on southwest visibility,'' *Atmos. Environ.* **15**, 1955–1969 (1981).
3. W. White and D. Patterson, ''On the relative contributions of NO_2 and particles to the color of smoke plumes,'' *Atmos. Environ.* **15**, 2097–2104 (1981).
4. G. Hänel, ''Computation of the extinction of visible radiation by atmospheric aerosol particles as a function of the relative humidity,'' *Aerosol Sci.* **3**, 377–386 (1972).
5. C. Seigneur et al., ''Temporal and Spatial Variability of the Visual Effects of Stack Plumes,'' EPA Report 600/3-85/039 (1985).
6. R. Haus, K. Schaefer, J. Hughes, J. Heland, and W. Bautzer, ''FTIS remote sensing of smoke stack and test flare emissions,'' *Air Pollution and Visibility Measurements, Proc. SPIE* **2506**, 45–54 (1994).
7. T. Higleman and L. Smith, ''Advanced plume analysis software for gas measurement,'' *Proc. SPIE Aerosense Conference* **2763**, 128–135 (1996).
8. N. Gat, S. Subramanian, J. Barhen, M. Sheffield, and H. Erives, ''Chemical detection using the airborne thermal infrared imaging spectrometer (TIRIS),'' *Proc. SPIE* **3082**, 156–164 (1997).
9. D. A. Haugan, *Lectures on Air Pollution and Environmental Impact*, American Meteorological Society (AMS), Boston, MA (1975).
10. J. Halitsky, ''A jet plume model for short stacks,'' *JPACA Note-Book* **39**, 856–858 (1989).
11. G. L. Stephens, ''Radiation profiles in extended water clouds II,'' *J. Atmos. Sci.* **35**, 2132 (1978).
12. R. M. Goody and Y. L. Yung, *Atmospheric Radiation*, Oxford University Press (1989).
13. R. W. Fenn et al., Chapter 18 in *Handbook of Geophysics and the Space Environment*, Air Force Geophysics Lab, Boston, MA (1985).
14. S. S. Penner, *Quantitative Molecular Spectroscopy and Gas Emissivities*, Addison Wesley (1959).
15. K. R. Westber et al., ''Chemical release rates during the first effluent tracking experiments at NTS,'' Aerospace Report No. ATR-95(9975)-5 (1996).
16. M. L. Polak, J. L. Hall, and H. C. Herr, ''Passive Fourier transform infrared spectroscopy of chemical plumes: An algorithm for quantitative interpretation and real-time background removal,'' *Appl. Opt.* **34**(24), 5406–5412 (1995).

S. Didi Kuo: Biography not available.

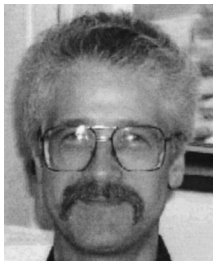

John R. Schott holds the Frederick and Anna B. Weidman Distinguished Professorship in the Chester F. Carlson Center for Imaging Science at the Rochester Institute of Technology where he heads the Digital Imaging and Remote Sensing Laboratory. He joined RIT in 1980 after eight years with Calspan Corporation where he was a principal physicist conducting remote sensing research for government and industrial sponsors. His research interest focuses on quantitative radiometric remote sensing and he has recently written a text/reference on this subject, *Remote Sensing: The Imaging Chain Approach.* Dr. Schott's ongoing research interest focuses on hyperspectral synthetic image generation, atmospheric propagation and correction and remote sensing on the Great Lakes.

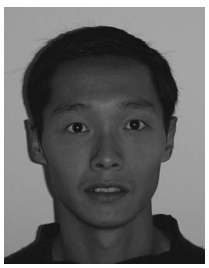

Chia Y. Chang received his BS in imaging science from the Rochester Institute of Technology and has been employed at the Digital Imaging and Remote Sensing Laboratory as a research assistant. His senior research involved the Evaluation of Inversion Algorithms on DIRSIG Generated Plume Model Simulations. He is currently employed at Photon Research Associates as a systems analyst.